Nanoscale Advances

ROYAL SOCIETY OF CHEMISTRY

PAPER

View Article Online
View Journal | View Issue

Cite this: *Nanoscale Adv.*, 2023, **5**, 2096

Nanowires exfoliated from one-dimensional van der Waals transition metal trihalides and quadrihalides†

Chuanxun Su *[ab] and Lixin He *[ab]

Received 1st December 2022
Accepted 1st March 2023

DOI: 10.1039/d2na00877g

rsc.li/nanoscale-advances

The exfoliation of van der Waals (vdW) materials has been widely used to fabricate two-dimensional (2D) materials. However, the exfoliation of vdW materials to isolate atomically thin nanowires (NWs) is an emerging research topic. In this letter, we identify a large class of transition metal trihalides (TMX_3), which have one-dimensional (1D) vdW structures, *i.e.*, they comprise columns of face-sharing TMX_6 octahedral chains, whereas the chains are bound by weak vdW forces. Our calculations show that the single-chain and multiple-chain NWs constructed from these 1D vdW structures are stable. The calculated binding energies of the NWs are relatively small, suggesting that it is possible to exfoliate NWs from the 1D vdW materials. We further identify several 1D vdW transition metal quadrihalides (TMX_4) that are candidates for exfoliation. This work opens a paradigm for exfoliating NWs from 1D vdW materials.

Introduction

The exfoliation of van der Waals (vdW) materials to isolate atomically thin films is widely used by experimentalists to produce two-dimensional (2D) materials.[1,2] The vdW materials that are successfully exfoliated can be natural or synthetic. First-principles calculations predicted a large number of vdW materials that can be exfoliated to build 2D materials by screening databases of crystal structures.[3–6] These data provide valuable guidance to experimentalists for discovering novel 2D materials.

One-dimensional (1D) vdW materials are made up of strongly bonded 1D atomic chains with weak inter-chain vdW forces. A previous experimental study verified the existence of vdW forces between atomic chains in 1D vdW material Tellurium by Raman spectroscopy.[7] It is possible that 1D vdW materials can be exfoliated into nanowires (NWs), which provides a top-down approach to fabricate NWs. Quantum effects will be strong in atomically thin NWs, which may host exotic physics. However, the research on the exfoliation of vdW materials down to atomically thin NWs is still very limited.[8] Freestanding atomically thin transition metal trihalide (TMX_3) NW structures have been reported to be stable by previous studies. For example, a recent theoretical study investigated the magnetic and electronic properties of 3d transition-metal tribromide NWs, *i.e.* $TMBr_3$ (TM = Sc, Ti, V, Cr, Co, and Cu), and half-metallicity was reported in ferromagnetic (FM) VBr_3 and $CuBr_3$ NWs.[9] Guo *et al.*[10] systematically studied vanadium-trihalide VX_3 (X= F, Cl, Br, I) NWs and found that a single-chain VI_3 NW is a FM semiconductor. The metal ions in TMX_3 may have local magnetic moments, which may host new physical phenomena and could be useful for future spintronic applications. However, these previously reported NWs do not have a corresponding 1D vdW bulk phase for exfoliation.

In this study, we present computational research on the exfoliation of 1D vdW TMX_3 and transition metal quadrihalides (TMX_4). We first show that TiI_3[11] is a 1D vdW material that can be exfoliated down to NWs consisting of a single chain or multiple chains of TiI_6 octahedra. We demonstrate that the NWs are thermodynamically stable. To find more exfoliable 1D vdW materials, we use the structure prototype analysis package (SPAP)[12] to search for structures that are similar to the TiI_3 structure prototype in the Crystallography Open Database (COD).[13] We identify a large class of 1D vdW TMX_3 materials, including β-$TiCl_3$,[14] $RuBr_3$,[15,16] β-$RuCl_3$,[15] $TcBr_3$,[17] $MoBr_3$,[16,18] and ZrI_3.[19] These 1D vdW materials all have relatively small binding energies and therefore are potentially exfoliable. We further examine the magnetism, stability, and electronic structures of the NWs. We also find a series of 1D vdW TMX_4 materials, including PtI_4,[20] $OsBr_4$,[21] $TcCl_4$,[22] TcF_4,[23] $ZrCl_4$,[24] $HfCl_4$,[25] TiI_4,[26] and UI_4,[27] which are candidates for exfoliation. This work opens a new path to fabricate NWs by a top-down approach.

[a]*CAS Key Laboratory of Quantum Information, University of Science and Technology of China, Hefei, 230026, Anhui, People's Republic of China. E-mail: sucx@ustc.edu.cn; helx@ustc.edu.cn*

[b]*Synergetic Innovation Center of Quantum Information and Quantum Physics, University of Science and Technology of China, Hefei, 230026, People's Republic of China*

† Electronic supplementary information (ESI) available: Method to query structures in the database, structure prediction for CrI_3, electronic band structure and density of states, phonon spectra, *ab initio* molecular dynamics simulations, and structures for the NWs and bulk *P*6_3/*mcm* CrI_3. See DOI: https://doi.org/10.1039/d2na00877g

Results and discussion

TiI_3 nanowires

As shown in Fig. 1, the orthorhombic low-temperature phase of TiI_3 (space group *Pmmn*)[11] comprises parallel infinite columns of face-sharing TiI_6 octahedra and the Ti atoms form dimers within the chains. In a unit cell, each chain contains 2 transition metal Ti atoms, which have a regular alternation of short and long inter-Ti distances as shown in Fig. 1(b). The TiI_3 structure is a typical 1D vdW material. We construct 1 chain, 3 chains, and 7 chains of freestanding NWs from orthorhombic bulk TiI_3, as shown in Fig. 2. The NW structures are then fully relaxed.

We use the coordination characterization function (CCF) to characterize the 1-chain TiI_3 NW. Details about the CCF are provided in the Methods section. For the 1-chain TiI_3 NW, the alternating short and long inter-Ti distances lead to alternating splitting and non-splitting peaks of $ccf^{static}_{Ti-Ti}(r)$ in Fig. 3. We define the pair function $P_{ij}(r_1,r_2)$ to characterize the number of atomic pairs for 2 formula units of TiI_3 within a certain range between r_1 and r_2, such that

$$P_{ij}(r_1,r_2) = \frac{2N}{n_{fu}} \int_{r_1}^{r_2} ccf_{ij}(r)dr, \quad (1)$$

where N is the number of atoms in the unit cell and n_{fu} denotes the number of formula units TiI_3 in the unit cell. As shown in Fig. 3, the $P^{static}_{Ti-Ti}(0.0,5.0)$ for $ccf^{static}_{Ti-Ti}(r)$ equals 2.0. This is contributed by 2 Ti atomic pairs, belonging to the same unit cell, with distances smaller than 5.0 Å. The 2 TiI_6 octahedra in the unit cell contribute to the first peak of $ccf^{static}_{Ti-I}(r)$ and $P^{static}_{Ti-I}(0.0,4.0) = 12.0$.

To determine the magnetic ground state of the NWs, we compare the total energies of different magnetic configurations for each NW structure. The total energies for various magnetic configurations are listed in Table S2 in the ESI.† All TiI_3 NWs are nonmagnetic (NM). We calculate the binding energy (per atom) of a NW relative to its bulk material as

$$E_b = \frac{E_{NW}}{N_{NW}} - \frac{E_{bulk}}{N_{bulk}}, \quad (2)$$

where E_{NW} and E_{bulk} are the total energies of the NW and 1D vdW bulk structures, respectively, and N_{NW} and N_{bulk} are the number of atoms in the NW and bulk unit cell, respectively. The calculated E_bs are listed in Table 1. The E_bs for the 1-chain, 3-chain, and 7-chain TiI_3 NWs are 0.1643, 0.1115, and 0.0725 eV per atom, respectively. The E_b decreases as the NW becomes thicker, because of the decrease in the surface-to-volume ratio. Previous studies suggest that monolayers with E_b smaller than 0.15 eV per atom may be feasible for exfoliation.[28–30] Since the mechanism of exfoliating a 1D NW from a bulk structure is similar to that of exfoliating a 2D layer, which requires breaking the weak vdW interactions, we believe that the criterion is also reasonable for 1D systems. However, experimental verification is required to confirm its validity.

To investigate the stability of the NWs, we recorded the phonon spectra of the 1-chain TiI_3 NW, and no imaginary phonon frequencies are found, which indicates that it is dynamically stable. Since 3- and 7-chain TiI_3 NWs have lower E_bs than 1-chain TiI_3 NWs, they are expected to be more stable. This expectation is supported by our phonon spectrum calculations (Fig. S5 in the ESI†). To further check the stability of the NWs at finite temperatures, we perform *ab initio* molecular dynamics (AIMD) simulations of the 1-chain NW at 300 K. We calculate the CCFs of 3168 structures taken from the AIMD trajectories in the time range between 0.5 and 10.0 ps, and the averaged CCFs are shown in Fig. 3. We see that the CCFs of the 1-chain TiI_3 at 300 K only have minor changes compared to those at zero temperature. The double-peak feature of CCFs is still preserved. The CCFs of Ti–I and I–I pairs are more smeared, and some double peaks merge into single peaks, which indicates that the I atoms move more vigorously. The platforms of ground state pair functions $P^{static}_{ij}(0,r)$ and $P^{AIMD}_{ij}(0,r)$ at 300 K

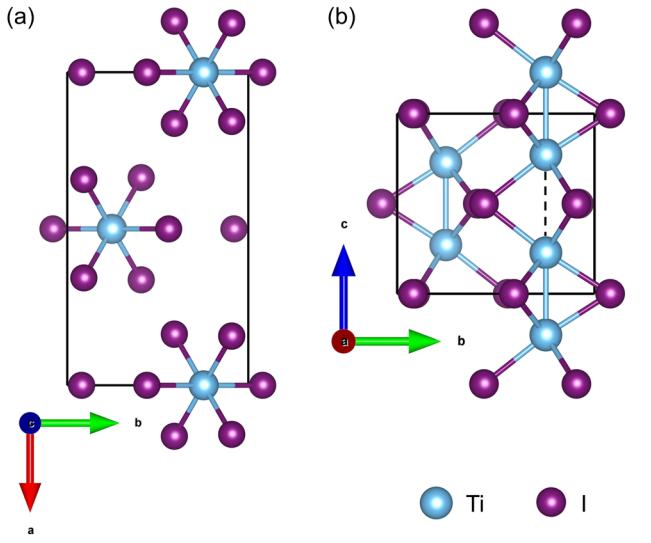

Fig. 1 The orthorhombic bulk structure *Pmmn* of TiI_3. (a) The chains of face-sharing TiI_6 octahedra run along the *c*-axis and are arranged in the *ab* plane. (b) The crystal structure looking through the *a*-axis. The blue solid sticks and dashed line indicate the short and long Ti–Ti bonds, respectively.

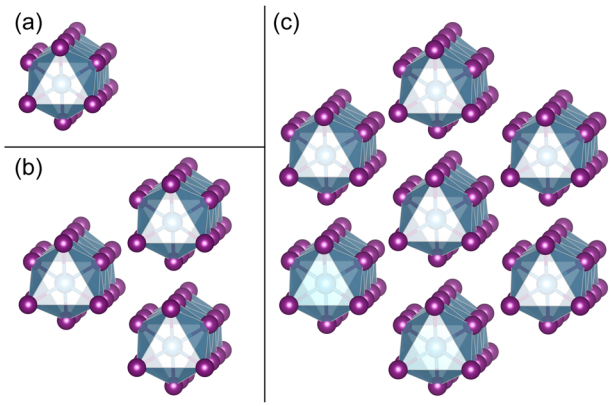

Fig. 2 (a)–(c) NWs consist of 1 chain, 3 chains, and 7 chains of face-sharing octahedra exfoliated from the bulk phase of TiI_3, respectively.

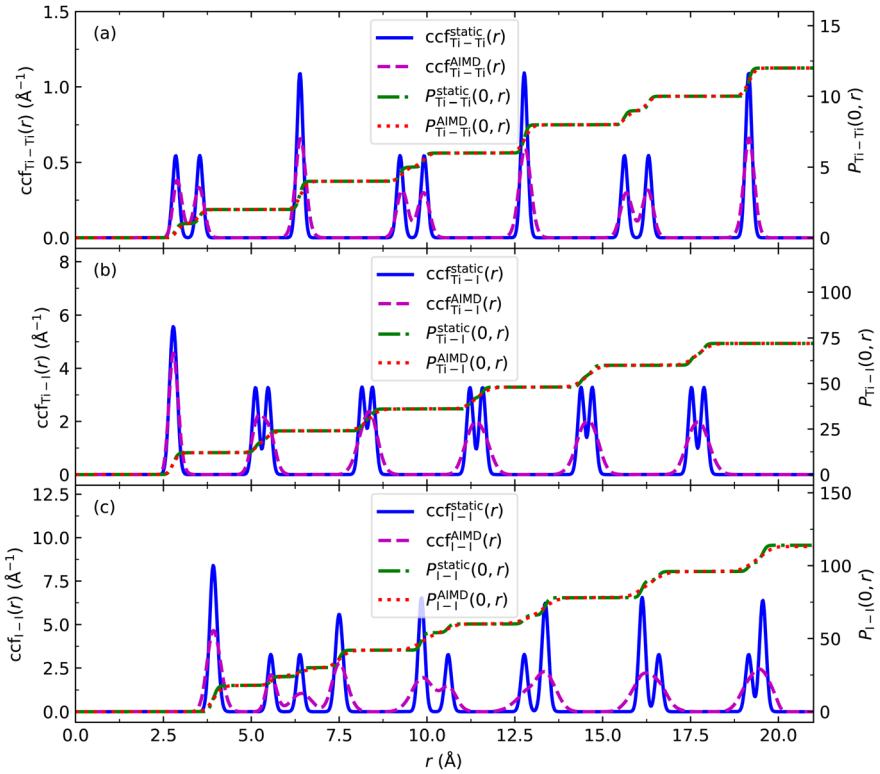

Fig. 3 The CCFs of the relaxed (static) 1-chain TiI_3 NW, $ccf_{ij}^{static}(r)$ and the averaged CCF, $ccf_{ij}^{AIMD}(r)$ of 1-chain TiI_3 NWs at 300 K for (a) Ti–Ti, (b) Ti–I, and (c) I–I pairs. The corresponding pair functions $P_{ij}^{static}(0,r)$ and $P_{ij}^{AIMD}(0,r)$ are also shown.

match very well. Importantly, the CCFs at 300 K still have the well organized periodicity, suggesting that the NW structure preserves the long range ordering (*i.e.*, the crystal structure).

TMX_3 nanowires

Since we have shown that TiI_3 is exfoliable to stable NWs, we aim to find more materials similar to TiI_3 for exfoliation, with

Table 1 List of physical properties of the 1D vdW bulk materials and the exfoliated NWs. E_b and M are the binding energies and projected magnetic moments for transition metals, respectively

Compound	Space group	System	E_b (eV per atom)	Magnetism	M (μ_B)	Band gap (eV)
TiI_3	*Pmmn*	Bulk		NM	0.0	0.1
TiI_3		1-Chain	0.1643	NM	0.0	0.3
TiI_3		3-Chain	0.1114	NM	0.0	0.2
TiI_3		7-Chain	0.0725	NM	0.0	0.2
β-$TiCl_3$	*Pmmn*	Bulk		NM	0.0	0.1
$TiCl_3$		1-Chain	0.1152	NM	0.0	0.2
$TiCl_3$		Monolayer	0.0792	NM	0.0	0.2
$MoBr_3$	*Pmmn*	Bulk		AFM	1.8	1.0
$MoBr_3$		1-Chain	0.1358	AFM	1.8	1.2
β-$RuCl_3$	*Pmmn*	Bulk		NM	0.0	0.1
$RuCl_3$		1-Chain	0.1153	NM	0.0	0.3
$RuBr_3$	*Pmmn*	Bulk		NM	0.0	0.1
$RuBr_3$		1-Chain	0.1342	NM	0.0	0.5
ZrI_3	*Pmmn*	Bulk		NM	0.0	0.0
ZrI_3		1-Chain	0.1636	NM	0.0	0.3
CrI_3	$P6_3/mcm$	Bulk		FM	3.4	0.1
CrI_3		1-Chain	0.1558	AFM	3.3	0.8
CrI_3		3-Chain	0.1068	FM	3.4	0.5
CrI_3		7-Chain	0.0697	FM	3.4	0.3
$TcBr_3$	*Pmmn*	Bulk		FM	0.9	0.1
$TcBr_3$		1-Chain	0.1421	FM	0.8	0.2
$TcBr_4$	*Pbca*	Bulk		AFM	2.1	0.6
$TcBr_4$		1-Chain	0.1394	AFM	2.2	0.9

even lower E_b and possibly being magnetic. We use the SPAP code[12] to calculate the structural distance (d) between the orthorhombic phase of (bulk) TiI_3 and structures with composition type AB_3 sourced from the COD.[13] The structures are first adjusted to an atom number density that is the same as that of the target TiI_3 structure, before calculating the d. The structural distance d is a dimensionless quantity which can be obtained by comparing the similarity of the CCFs of the structures. The detailed methodology is introduced in the ESI.† A structure with smaller d is more similar to the target structure. We select 1153 AB_3 structures from the COD and calculate the structural distances between the TiI_3 structure and the adjusted AB_3 structures. The structures are ordered by the increase in the structural distance, and the first 42 structures are listed in Table 2. Usually, structures with distances smaller than 0.075 in this framework are regarded as similar structures. We identity a series of 1D vdW materials that have structural distances smaller than 0.100 with TiI_3, including β-$TiCl_3$,[14] $RuBr_3$,[15,16] β-$RuCl_3$,[15] $TcBr_3$,[17] $MoBr_3$,[16,18] and ZrI_3.[19]

We construct NWs from the 1D vdW bulk structures found in the database. The space group of the bulk materials, the NW binding energy E_b, the magnetic ground state, the magnetic moments of transition metals, *etc.*, are listed in Table 1. The 1-chain $TiCl_3$, $MoBr_3$, $RuCl_3$, $RuBr_3$, and $TcBr_3$ NWs have E_b below 0.1500 eV per atom, indicating that they are likely to be exfoliated in experiments. Among them, the 1-chain $TiCl_3$ NW has the lowest E_b of 0.1152 eV per atom, which is most promising for synthesis. The low E_b of monolayer $TiCl_3$ (0.0792 eV per atom) indicates that the monolayer can also be obtained by exfoliation. Even if some freestanding NWs cannot be synthesized, they still have the possibility to stabilize on substrates.

Table 2 The structural distance between the orthorhombic low-temperature (below 100 K) phase of TiI_3 and the adjusted AB_3 structures from the COD[a]

Compound	No.	d	Compound	No.	d
TiI_3	1	0.000	CrF_3	22	0.112
$MoBr_3$	2	0.021	RhF_3	23	0.113
TiI_3	3	0.032	Fe_3N	24	0.119
$RuBr_3$	4	0.039	Zr_3O	25	0.122
ZrI_3	5	0.043	ReO_3	26	0.123
$RuBr_3$	6	0.044	IrF_3	27	0.132
$MoBr_3$	7	0.056	BiI_3	28	0.133
$TiCl_3$	8	0.060	CrF_3	29	0.135
$RuCl_3$	9	0.063	Fe_3N	30	0.141
$RuBr_3$	10	0.065	FeF_3	31	0.142
$RuBr_3$	11	0.069	PdF_3	32	0.147
YI_3	12	0.074	FeF_3	33	0.151
$RuBr_3$	13	0.075	Fe_3N	34	0.152
$TcBr_3$	14	0.076	CrF_3	35	0.156
$RuCl_3$	15	0.079	CrF_3	36	0.161
BiI_3	16	0.082	FeF_3	37	0.165
Zr_3O	17	0.091	CrF_3	38	0.165
$ScCl_3$	18	0.100	Ni_3C	39	0.169
Ti_3O	19	0.102	FeF_3	40	0.174
SbI_3	20	0.104	$TiCl_3$	41	0.198
RuF_3	21	0.106	$TiCl_3$	42	0.205

[a] The structures are sorted in the ascending order of distances. No. represents the sequence number of the structure. Only the first 42 structures are listed.

Since the FM monolayer CrI_3 was successfully fabricated in 2017,[31] this material has gained growing attention. However, the ground state structure of CrI_3 (rhombohedral structure, space group $R\bar{3}$, BiI_3 structure type)[32] is not of the 1D vdW structure. To check whether CrI_3 may have a meta-stable 1D vdW structure, we perform structure prediction calculations, which use the crystal structure prototype database to generate candidate structures.[12] The details of this method are given in the ESI.† The structure with the lowest energy among the predicted structures is the experimental $R\bar{3}$ structure. However, we find a meta-stable structure with the space group $P6_3/mcm$, which is only 0.0352 eV per atom higher than the $R\bar{3}$ structure, consisting of face-sharing CrI_6 octahedral chains. Phonon spectra calculation shows that the $P6_3/mcm$ CrI_3 is dynamically stable. The structure is similar to that of the high temperature phase of TiI_3, and is of the 1D vdW structure type. The $P6_3/mcm$ CrI_3 structure is also FM. We calculate the binding energies of the CrI_3 NWs constructed from the $P6_3/mcm$ CrI_3 structures, and the results are given in Table 1. The E_b of the 1-chain CrI_3 NW is approximately 0.156 eV per atom, and the E_b decreases as the NW becomes thicker, as expected.

Table 1 also shows the calculated magnetism of these materials. TiI_3, $TiCl_3$, $RuCl_3$, $RuBr_3$, and ZrI_3 are NM for both bulk and NW phases. The NWs and bulk $MoBr_3$ are antiferromagnetic (AFM) and the projected magnetic moment for Mo is 1.8 μ_B. The $TcBr_3$ system turns out to be FM. Interestingly, the thickness of the NW may change its magnetism. For example, the bulk, 3-chain, and 7-chain CrI_3 are FM, whereas the 1-chain CrI_3 is AFM. The change of magnetism through the thickness of a 1D material provides an effective way to tune the magnetism of NWs.

The electronic band structure and density of states calculations show that all the TMX_3 NWs are semiconductors. The band gaps of the NWs are listed in Table 1 compared to that of the bulk phase. The 1-chain $MoBr_3$ has the largest band gap of 1.2 eV, whereas the 3- and 7-chain TiI_3, 1-chain $TiCl_3$, and 1-chain $TcBr_3$ have the smallest band gap of 0.2 eV. The increase in the thickness of a NW reduces its band gap, due to quantum confinement effects. For example, 1-chain and 3-chain TiI_3 have band gaps of 0.3 and 0.2 eV, respectively, and the band gaps for 1-chain, 3-chain, and 7-chain CrI_3 NWs are 0.8, 0.5, and 0.3 eV, respectively. The bulk 1D vdW TMX_3 has smaller band gaps compared to its respective NWs. In particular, the metallic bulk ZrI_3 transforms to a semiconductor in the 1-chain NW.

To verify the dynamic and thermodynamic stabilities of the freestanding NWs, we recorded the phonon spectrum and performed AIMD simulations. The 1-chain TiI_3, $TiCl_3$, $MoBr_3$, $RuCl_3$, CrI_3, and 3-chain CrI_3, TiI_3, and 7-chain TiI_3 NWs have no or negligible imaginary phonon frequencies, indicating that they are dynamically stable. The phonon spectra of 1-chain $RuBr_3$, ZrI_3, and $TcBr_3$ NWs have slightly softened modes near the Γ point (see the ESI†). However, the AIMD simulations show that all these NWs are thermodynamically stable at 300 K. The 1-chain $RuBr_3$, ZrI_3, and $TcBr_3$ NWs are presumably stabilized by the free energy at room temperature (Fig. S7 and S8 in the ESI†).

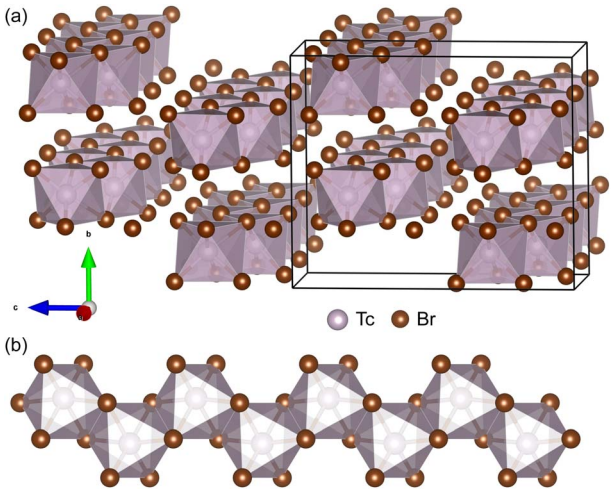

Fig. 4 (a) The experimental bulk phase *Pbca* of $TcBr_4$ viewed along the chains of edge-sharing $TcBr_6$ octahedra. (b) 1 chain of $TcBr_4$ exfoliated from its bulk phase.

1D vdW TMX_4 materials

In addition to TMX_3 materials, we also find a series of 1D vdW TMX_4 materials that are potentially exfoliable into NWs. Bulk $TcBr_3$ and $TcBr_4$ were synthesized by reaction between technetium metal and bromine and characterized by single crystal XRD.[17] Interestingly, both $TcBr_3$ and $TcBr_4$ are 1D vdW materials. As shown in Fig. 4(a), the $TcBr_4$ comprises chains of edge-sharing $TcBr_6$ octahedra. The $TcBr_4$ atomic chains are bonded through weaker inter-chain vdW forces in the *bc* plane. We exfoliate the freestanding $TcBr_4$ NWs, presented in Fig. 4(b), from its bulk phase. The low binding energy (0.1394 eV per atom) verifies that the $TcBr_4$ NW is exfoliable. The AIMD simulations at 300 K show that the NW is thermodynamically stable. The bulk and NW structures of $TcBr_4$ are both AFM. Using the SPAP to search structures similar to bulk $TcBr_4$ in the COD, we find more 1D vdW materials, including TcF_4, $TcCl_4$, $ZrCl_4$, $HfCl_4$, $OsBr_4$, TiI_4, PtI_4, and UI_4. These materials are all potentially exfoliable to produce NWs. We leave these materials for future investigations.

Conclusion

We identify a large class of TMX_3 materials (TiI_3, β-$TiCl_3$, $RuBr_3$, β-$RuCl_3$, $TcBr_3$, $MoBr_3$, ZrI_3, *etc.*), which have 1D vdW structures and are exfoliable to NWs, using first-principles calculations. Our calculations show that the single-chain and multiple-chain NWs constructed from these 1D vdW structures are stable. The calculated binding energies of the NWs are relatively small, which is promising for exfoliation. We further identify several 1D vdW TMX_4 materials which are candidates for exfoliation. This work opens a top-down approach to fabricate NWs from 1D vdW materials.

Methods

Computational details

The first-principles calculations are performed within density functional theory using the projector augmented wave pseudopotentials[33,34] as implemented in the Vienna *ab initio* simulation package.[35] We utilize the optimized exchange van der Waals functional B86b of the Becke (optB86b vdW) functional to handle the effect of van der Waals interactions.[36] An energy cutoff of 500 eV is applied in the expansion of the wave function into plane waves, and Monkhorst–Pack k point meshes with a grid smaller than 0.2 $Å^{-1}$ are used to sample the Brillouin zone. For the NW calculations, we leave a vacuum space larger than 16 Å around the NWs to eliminate the fictitious interactions between the NW and its periodic images. The structures are relaxed until the forces are less than 1 meV $Å^{-1}$. For compounds with Ru and Cr elements, we use the DFT + U method.[37] We use $U = 3.5$ eV and $J = 1.0$ eV for Ru element, in which the relaxed bulk β-$RuCl_3$ and $RuBr_3$ structures are close to the experimental structures. We use $U = 3.9$ eV and $J = 1.1$ eV for Cr.[38] AIMD simulations are performed with a supercell, which is extended 4 times the unit cell along the atomic chain, at 300 K for 10 ps. The phonon spectra are recorded using a supercell approach[39] implemented in the PHONOPY package.[40] We use the VESTA code to visualize structural images.[41]

Coordination characterization function

The CCF identifies the fingerprint of a structure on the basis of its interatomic distances. For pairs of atomic types i and j,

$$\mathrm{ccf}_{ij}(r) = \left(1 - \frac{1}{2}\delta_{ij}\right) \frac{1}{N} \sum_{n_i} \sum_{n_j} f\left(r_{n_i n_j}\right) \sqrt{\frac{a_{\mathrm{pw}}}{\pi}} \exp\left(-a_{\mathrm{pw}}\left(r - r_{n_i n_j}\right)^2\right), \quad (3)$$

where N is the number of atoms in the unit cell, n_i runs over all the atoms of the ith type within the unit cell, and n_j runs over all the atoms of the jth type within the extended cell, $f(r_{n_i n_j})$ is the weighting function for different interatomic distances, $r_{n_i n_j}$ is the interatomic distance less than the cutoff radius r_{cut}, and a_{pw} (usually 60.0 $Å^{-2}$) is a parameter that controls the spread of the normalized Gaussian function $\sqrt{a_{\mathrm{pw}}/\pi}\exp(-a_{\mathrm{pw}}(r - r_{n_i n_j})^2)$. We use $f(r_{n_i n_j}) = 1$ and $r_{\mathrm{cut}} = 20$ Å for the calculation of CCFs shown in Fig. 3.

Structure prototype analysis package

The SPAP[12] analyzes symmetry and compares the similarity of different atomic structures. It can cluster a large number of atomic structures according to the physical features, such as symmetry, composition type, and structural distance. The SPAP allows us to find structures in the database that are similar to the target structure. The detailed method of the SPAP can be found in the ESI.†

Author contributions

Chuanxun Su: conceptualization, calculation, data curation, software, and writing – original draft. Lixin He: supervision, validation, funding acquisition, and writing – review & editing.

Conflicts of interest

The authors declare no competing financial interest.

Acknowledgements

This work was funded by the Chinese National Science Foundation (No. 12134012). The numerical calculations were performed on the USTC HPC facilities.

References

1 K. S. Novoselov, A. K. Geim, S. V. Morozov, D.-e. Jiang, Y. Zhang, S. V. Dubonos, I. V. Grigorieva and A. A. Firsov, *Science*, 2004, **306**, 666–669.
2 R. Frisenda, Y. Niu, P. Gant, M. Muñoz and A. Castellanos-Gomez, *npj 2D Mater. Appl.*, 2020, **4**, 1–13.
3 S. Lebègue, T. Björkman, M. Klintenberg, R. M. Nieminen and O. Eriksson, *Phys. Rev. X*, 2013, **3**, 031002.
4 N. Mounet, M. Gibertini, P. Schwaller, D. Campi, A. Merkys, A. Marrazzo, T. Sohier, I. E. Castelli, A. Cepellotti, G. Pizzi, et al., *Nat. Nanotechnol.*, 2018, **13**, 246–252.
5 Y. Zhu, X. Kong, T. D. Rhone and H. Guo, *Phys. Rev. Mater.*, 2018, **2**, 081001.
6 P. M. Larsen, M. Pandey, M. Strange and K. W. Jacobsen, *Phys. Rev. Mater.*, 2019, **3**, 034003.
7 Y. Du, G. Qiu, Y. Wang, M. Si, X. Xu, W. Wu and P. D. Ye, *Nano Lett.*, 2017, **17**, 3965–3973.
8 Y. Zhu, D. A. Rehn, E. R. Antoniuk, G. Cheon, R. Freitas, A. Krishnapriyan and E. J. Reed, *ACS Nano*, 2021, **15**, 9851–9859.
9 S.-s. Li, Y.-p. Wang, S.-j. Hu, D. Chen, C.-w. Zhang and S.-s. Yan, *Nanoscale*, 2018, **10**, 15545–15552.
10 Z. Guo, Q. Chen, J. Yuan, K. Xia, X. Wang and J. Sun, *J. Phys. Chem. C*, 2019, **124**, 2096–2103.
11 J. Angelkort, A. Schönleber and S. van Smaalen, *J. Solid State Chem.*, 2009, **182**, 525–531.
12 C. Su, J. Lv, Q. Li, H. Wang, L. Zhang, Y. Wang and Y. Ma, *J. Phys.: Condens. Matter*, 2017, **29**, 165901.
13 S. Gražulis, A. Daškevič, A. Merkys, D. Chateigner, L. Lutterotti, M. Quiros, N. R. Serebryanaya, P. Moeck, R. T. Downs and A. Le Bail, *Nucleic Acids Res.*, 2012, **40**, D420–D427.
14 G. Natta, P. Corradini and G. Allegra, *J. Polym. Sci.*, 1961, **51**, 399–410.
15 H. Hillebrecht, T. Ludwig and G. Thiele, *Z. Anorg. Allg. Chem.*, 2004, **630**, 2199–2204.
16 S. Merlino, L. Labella, F. Marchetti and S. Toscani, *Chem. Mater.*, 2004, **16**, 3895–3903.
17 F. Poineau, E. E. Rodriguez, P. M. Forster, A. P. Sattelberger, A. K. Cheetham and K. R. Czerwinski, *J. Am. Chem. Soc.*, 2009, **131**, 910–911.
18 D. Babel, *J. Solid State Chem.*, 1972, **4**, 410–416.
19 A. Lachgar, D. S. Dudis and J. D. Corbett, *Inorg. Chem.*, 1990, **29**, 2242–2246.
20 K. Brodersen, G. Thiele and B. Holle, *Z. Anorg. Allg. Chem.*, 1969, **369**, 154–160.
21 G. Thiele, H. Wochner and H. Wagner, *Z. Anorg. Allg. Chem.*, 1985, **530**, 178–186.
22 M. Elder and B. R. Penfold, *Inorg. Chem.*, 1966, **5**, 1197–1200.
23 P. F. Weck, E. Kim, F. Poineau, E. E. Rodriguez, A. P. Sattelberger and K. R. Czerwinski, *Inorg. Chem.*, 2009, **48**, 6555–6558.
24 R. Borjas Nevarez, S. M. Balasekaran, E. Kim, P. Weck and F. Poineau, *Acta Crystallogr., Sect. C: Struct. Chem.*, 2018, **74**, 307–311.
25 R. Niewa and H. Jacobs, *Z. Krystallog.*, 1995, **210**, 687.
26 S. Troyanov, *Zh. Neorg. Khim.*, 1993, **38**, 226–229.
27 J. Levy, J. Taylor and A. Waugh, *Inorg. Chem.*, 1980, **19**, 672–674.
28 A. K. Singh, K. Mathew, H. L. Zhuang and R. G. Hennig, *J. Phys. Chem. Lett.*, 2015, **6**, 1087–1098.
29 B. C. Revard, W. W. Tipton, A. Yesypenko and R. G. Hennig, *Phys. Rev. B*, 2016, **93**, 054117.
30 M. Ashton, J. Paul, S. B. Sinnott and R. G. Hennig, *Phys. Rev. Lett.*, 2017, **118**, 106101.
31 B. Huang, G. Clark, E. Navarro-Moratalla, D. R. Klein, R. Cheng, K. L. Seyler, D. Zhong, E. Schmidgall, M. A. McGuire, D. H. Cobden, et al., *Nature*, 2017, **546**, 270–273.
32 M. A. McGuire, H. Dixit, V. R. Cooper and B. C. Sales, *Chem. Mater.*, 2015, **27**, 612–620.
33 P. E. Blöchl, *Phys. Rev. B: Condens. Matter Mater. Phys.*, 1994, **50**, 17953.
34 G. Kresse and D. Joubert, *Phys. Rev. B: Condens. Matter Mater. Phys.*, 1999, **59**, 1758.
35 G. Kresse and J. Furthmüller, *Phys. Rev. B: Condens. Matter Mater. Phys.*, 1996, **54**, 11169.
36 J. Klimeš, D. R. Bowler and A. Michaelides, *Phys. Rev. B: Condens. Matter Mater. Phys.*, 2011, **83**, 195131.
37 S. L. Dudarev, G. A. Botton, S. Y. Savrasov, C. Humphreys and A. P. Sutton, *Phys. Rev. B: Condens. Matter Mater. Phys.*, 1998, **57**, 1505.
38 P. Jiang, C. Wang, D. Chen, Z. Zhong, Z. Yuan, Z.-Y. Lu and W. Ji, *Phys. Rev. B*, 2019, **99**, 144401.
39 K. Parlinski, Z. Li and Y. Kawazoe, *Phys. Rev. Lett.*, 1997, **78**, 4063.
40 A. Togo and I. Tanaka, *Scr. Mater.*, 2015, **108**, 1–5.
41 K. Momma and F. Izumi, *J. Appl. Crystallogr.*, 2011, **44**, 1272–1276.